Compensation of Confounding T1 and T2 Dipolar and Residual Susceptibility Effects in DSC-MRI using Dual-Echo SPIRAL

E. S. Paulson[1], D. E. Prah[1], and K. M. Schmainda[1,2]

[1]Department of Biophysics, Medical College of Wisconsin, Milwaukee, WI, United States, [2]Department of Radiology, Medical College of Wisconsin, Milwaukee, WI, United States

Introduction. The use of paramagnetic gadolinium chelates in dynamic susceptibility contrast (DSC) MRI has been shown to exhibit different effects on signal intensity depending on the status of the local microenvironment. In the *presence* of an intact blood brain barrier (BBB) a highly concentrated bolus of gadolinium will remain compartmentalized to the vasculature, such that a magnetic susceptibility gradient is established between intra- and extravascular spaces resulting in signal decreases due to spin dephasing [1]. In addition to the transient signal decreases that occur during the bolus passage, a residual susceptibility-induced post-bolus signal attenuation is often observed. This may be attributed to an increased steady-state concentration of the contrast agent or binding of the agent to the walls of the vasculature [2]. In the *absence* of an intact BBB, some fraction of the bolus will extravasate into the extravascular extracellular space (EES) where dipole/dipole interactions between gadolinium's unpaired electrons and local tissue water protons will cause T1 and T2 shortening. T1 shortening results in signal enhancement that competes with the susceptibility-induced signal decrease whereas T2 shortening results in signal attenuation beyond the susceptibility-induced signal decrease. Both of these effects can confound perfusion estimates obtained with DSC-MRI [3,4]. Several methods have been developed to correct the confounding T1 effects, including post-processing correction [5], low flip angle acquisition [6], pre-enhancing tissue with a loading dose [7], and dual-echo acquisition [8-12]. However, the dipolar T2 and residual susceptibility effects are rarely compensated for [13]. We demonstrate here that the combination of a dual-echo, single-shot SPIRAL acquisition and post-processing algorithm can correct DSC-MRI time courses for both the dipolar T1 and T2 effects as well as residual susceptibility effects.

Methods. A prospective study was performed on nine patients with intracranial tumors that underwent rCBV analysis. Acquisition was performed on a 1.5T GE CV scanner (GE Healthcare, Milwaukee, Wisconsin) equipped with 4 G/cm gradients and a commercial 8-channel phased array RF coil. Perfusion weighted images were acquired using a single-shot, dual-echo, GRE-SPIRAL-out sequence with the following parameters: FOV=24 cm^2, matrix=64x64, slice thickness=5 mm, skip=1.5 mm, TE_1=3.3 msec, TE_2=30 msec, TR=1000 msec, number of slices=12, number of samples (reps)=180. A standard dose of Gadodiamide (0.1 mmol/kg, Omniscan) was injected at the 60th time point using a power injector. Post-contrast T1W images were then acquired using a conventional SE sequence over the same slice prescription with the following parameters: TE/TR/Matrix/NEX=10/450/256^2/2.

Data analysis was performed offline using AFNI and additional programs developed at our institution. Dynamic MR signal time courses from the second (more strongly T2*-weighted) echo were converted into concentration-time curves (i.e., $\Delta R2^*(t)$) in the usual manner via Equation 1 [3,4,6,7]. Note that these concentration-time curves can be contaminated by residual susceptibility and/or dipolar T1 and T2 effects. Correction of T1 leakage effects is achieved by taking the ratio of the second to first echo images at each time point as shown in Equation 2 [8-12]. Note that these concentration-time curves can still be confounded by residual susceptibility and/or dipolar T2 effects. Estimation of the magnitude of the dipolar T2 or residual susceptibility effects is accomplished by fitting a model to the concentration-time curves that accounts for the first pass and residual susceptibility or dipolar T2 effects as shown in Equation 3, where k, t_0, α, and β are the fit parameters for a gamma-variate function, and h is used to scale the cumulative integral of the gamma-variate function to the residual post-bolus baseline value [14]. As shown in Equation 4, concentration-time curves corrected for dipolar T1 and T2 and residual susceptibility effects are then generated by constructing a gamma-variate with the model parameters obtained from Equation 3. To compare the methods, estimates of rCBV were obtained by integrating over the first 120 time points of each $\Delta R2^*(t)$ (i.e., Equations 1, 2, and 4) using trapezoidal integration and then normalizing the rCBV estimates to the mean rCBV value obtained from ROIs drawn within normal appearing white matter.

$$[1]\quad \Delta R_2^*(t)_{+T_1,T_2} = -\frac{1}{TE}\ln\left(\frac{S(t)}{S_0}\right) \qquad [2]\quad \Delta R_2^*(t)_{+T2} = \frac{1}{(TE_1 - TE_2)}\ln\left(\frac{S_{TE_2}(t)}{S_{TE_1}(t)}\cdot\frac{S_{TE_{10}}}{S_{TE_{20}}}\right)$$

$$[3]\quad \Delta R_2^*(t)' = k(t-t_0)^{\alpha}e^{-\frac{(t-t_0)}{\beta}} + h\int_0^t k(t'-t_0)^{\alpha}e^{-\frac{(t'-t_0)}{\beta}}dt' \qquad [4]\quad \Delta R_2^*(t) = k(t-t_0)^{\alpha}e^{-\frac{(t-t_0)}{\beta}}$$

Figures 1-4: Descending rows, and left-right columns, represent Figures 1-4 and **a** and **b**, respectively. Please see text for details.

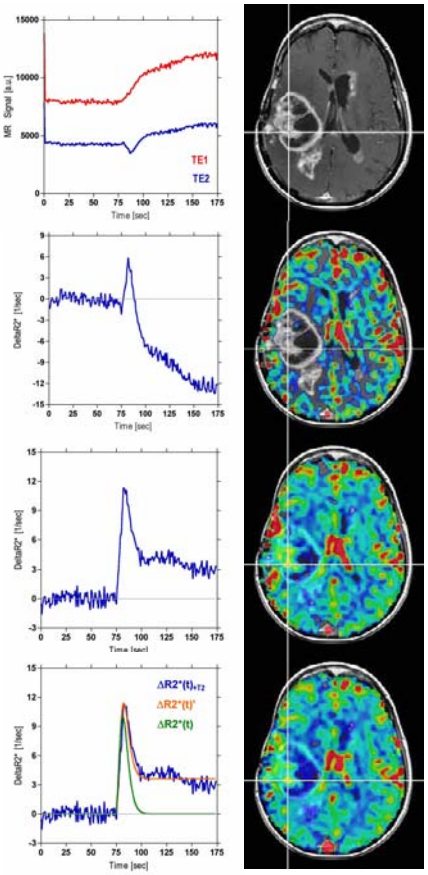

Results and Discussion. Figure 1a displays the raw time series of both echoes for the tumor voxel depicted on the post-contrast T1W anatomical image shown in Figure 1b. Extravasation of contrast agent is apparent from the increase in signal intensity in both echo time series (i.e., TE1 and TE2) during and following the arrival of the bolus. Figures 2a and b display a representative $\Delta R2^*(t)_{+T1,T2}$ curve obtained from Equation 1 and a corresponding rCBV map. Note that T1 leakage effects cause the post-bolus $\Delta R2^*$ to fall below the pre-bolus baseline, resulting in an underestimation of rCBV. This effect is apparent by a lack of blood volume in Figure 2b, which is exacerbated in regions of tumor. Figures 3a and b display a representative $\Delta R2^*(t)_{+T2}$ curve obtained from Equation 2 and a corresponding rCBV map. Note that the curve shown in Figure 3a has been corrected for T1 leakage effects, however dipolar T2 effects still exist (evident from the elevated post-bolus baseline). While correction for T1 effects prevents the underestimation of rCBV, an overestimation of rCBV can result from the residual susceptibility or dipolar T2 effects. Figures 4a and b display representative $\Delta R2^*(t)'$ (orange) and $\Delta R2^*(t)$ (green) curves obtained using Equations 3 and 4, and a corresponding rCBV map from Equation 4. Note that the green curve shown in Figure 4a, and rCBV map in Figure 4b have been corrected for T1 and T2 dipolar and residual susceptibility effects. This results in lower rCBV values seen in Figure 4b relative to Figure 3b, most notably in tumor, a result we contend should be more representative of the true blood volume.

The SPIRAL-based dual-echo approach described here offers some important advantages for DSC-MRI studies. While previous methods for simultaneously acquiring dual echo time courses have relied on keyhole acquisitions [8, 11, 12] or segmented echo-planar imaging [10, 12], SPIRAL reduces readout times by eliminating the filling of unused data in the corners of k-space and consequently, permits an increased slice number, increased resolution, or shorter TR capabilities.

These results suggest that a dual-echo acquisition method, which compensates for T1 leakage effects, combined with a post-processing algorithm for correcting dipolar T2 and residual susceptibility effects may be a superior method of performing DSC-MRI studies in brain tumors. Future work will include sequence parameter optimization, the collection of pre-contrast T1 maps along with the dual-echo data to facilitate calculation of the volume transfer constant, K^{trans}, and EES volume fraction, v_e, corrected for dipolar T2 and residual susceptibility effects [13], and an independent validation of the newly described method.

References. 1. Rosen et al., MRM 14:249-265 (1990), 2. Levin et al., MRM 34:655-663 (1995), 3. Kassner et al., JMRI 11:103-113 (2000), 4. Boxerman et al., AJNR 27(4):857-867 (2006), 5. Weisskoff et al., Proc. 2nd An. Soc. Mag. Reson. Med. (1994), 6. Donahue et al., MRM 43:845-853 (2000), 7. Knopp et al., Radiology 211:791-798 (1999), 8. Miyati et al., JMRI 7:230-235 (1997), 9. Li et al., Proc ISMRM 6th (1998), 10. Vonken et al., MRM 43:820-827 (2000), 11. Kim et al., MRI 22:307-314 (2004), 12. Zaitsev et al., Phys Med & Biol 50:4491-4505 (2005), 13. Quarles et al., Proc ISMRM 13th (2005), 14. Johnson et al., MRM 51:961-968 (2004).

Acknowledgements. Thanks to Eric C. Wong, Ph.D., M.D. for providing the original custom pulse sequence used in this study. This work was supported by NIH/NCI and GCRC grants CA082500 and M01-4400058, respectively.